The optimum Ga-67-citrate gamma camera imaging quality factors as first calculated and shown by the Taguchi's analysis

Da Ming Yeh[1,2,3] MD,
Pai Jung Chang[4] MSc,
Lung Kwang Pan[1] PhD

1. Graduate Institute of Radiological Science, Central Taiwan University of Science and Technology, Takun, Taichung 406, Taiwan
2. Department of Diagnostic Radiology, Chung Shan Medical University Hospital, Taichung, 402, Taiwan
3. School of Medical Imaging and Radiological Science, Chung Shan Medical University, Taichung, 402, Taiwan
4. Division of Nuclear Medical, Chung Shan Medical University Hospital, Taichung 402, Taiwan

***

Keywords: Image optimization
- Quality characteristics
- Gamma camera image
- Dominant factor from scanning
- Cross interaction factor

Correspondence address:
Prof. Lung Kwang Pan,
Department of Medical Imaging and Radiological Science,
Central Taiwan University of Science and Technology
TaKun, TaiChung 406, Taiwan, R.O.C.
Tel:(o) 886-4-2239-1647 ext. 7109
(m) 886-920-810-713
Fax: 886-4-2239-6762
E-mail: lkpan@ctust.edu.tw

Received:
27 February 2013
Accepted revised:
15 March 2013

Abstract

In this work gallium-67 (^{67}Ga) gamma camera imaging quality was optimized using the Taguchi's analysis and a planar phantom. *The acrylic planar phantom was LASER-cut* to form groups of slits 1mm wide and 5mm deep, to determine the spatial resolution and contrast ratio that could be achieved in a ^{67}Ga citrate nuclear medicine examination. The ^{67}Ga-citrate solution was injected into the slits to form an active radioactive line source which was placed between regular acrylic plates for optimization. Then, nine combinations of four operating factors: $L_9(3^4)$, of the gamma camera imaging system were used and followed the Taguchi's analysis. The four operating factors were: a) the type of collimator in front of the NaI(Tl) detector, b) the region of interest of ^{67}Ga gamma rays spectrum, c) the scanning speed of NaI(Tl) detector head and d) the activity of ^{67}Ga. The original judged grade of the planar phantom image quality was increased 36% and factors a) and b) were confirmed to dominate. The cross interaction among factors was also discussed. *Our results showed* that the optimal factor settings of the gamma camera imaging system were verified by performing a routine nuclear medicine examination in ten cases. Nine cases showed the same optimal settings as estimated by three highly trained radio-diagnostic physicians. Additionally, the optimal settings yielded clearer images with greater contrast than did the conventional settings. *In conclusion*, this work suggests for practical use, an optimized process for determining both the spatial resolution and the contrast ratio of a gamma camera imaging system using Taguchi's optimal analysis and a planar phantom. The Taguchi's method is most effective in targeting a single quality characteristic but can also be extended to satisfy multiple requirements under specific conditions by revising the definition of signal to noise ratio.

Hell J Nucl Med 2013; 16(1): 25-32 *Epub ahead of print: 26-3-2013* *Published on line:10 April 2013*

Introduction

Gamma camera imaging system has been widely used for diagnosis of various diseases, especially various carcinomas and tumor tissues. Rapid and simple imaging acquisition and post-processing methods improve diagnosis. However, for many nuclear medicine facilities the spatial resolution and contrast ratio are problems to be considered. An efficient method in defining spatial resolution and contrast ratio is essential [1-4]. A well designed phantom not only provides quantitative information that supports practical evaluation but also ensures clinical reproducibility of the optimized process for lymphomas, hepatic tumors and melanomas [5].

In this paper we propose a technique using a planar phantom for optimizing spatial resolution and for the contrast ratio of a gamma camera imaging system using Taguchi's optimal analysis and a planar phantom, which helps effectively in quantifying the performance of medical imaging system. The Taguchi's analysis was successfully applied to the optimization of medical imaging, while it has already gained reputation in many industrial fields.

Materials and methods

Taguchi's analysis

Taguchi's method is a very effective means of designing a high-quality system. Taguchi's method exploits unique orthogonal arrays to obtain extensive data from only a few experiments. The obtained optimal gamma camera settings are independent from environmental conditions and other factors. A statistical analysis of variance (ANOVA) was performed to identify factors that significantly affect the target variable signal to noise (S/N) and ANOVA analyses were combined to determine the optimal combination of

values of operating factors of the gamma camera imaging system [6, 7].

Orthogonal arrays

Unlike other analytical methods of optimization, Taguchi's method determines both the optimal value of a chosen factor from a finite set of analytical data and also the factors that dominate the target variable. This method has been widely utilized in precision manufacturing [8, 9] and other industrial fields and is applicable to nuclear medicine because of its efficient evaluation in identifying either dominant or minor factors in nuclear medicine examinations [10]. In this work, the four operating factors of the gamma camera imaging system used were the type of collimator, the region of interest (ROI) of the detected gamma ray spectrum, the scanning speed of the NaI(Tl) detector head and the activity of gallium-67 (^{67}Ga) radionuclide. Each of these factors can be assigned to three levels, therefore, a total of 81 (3X3X3X3) combinations were considered. By Taguchi's method, samples were organized into only nine Groups, which were used to obtain results with the same confidence as if they were to be considered in a conventional thorough optimization process [6]. Table 1 presents a standard L_9 (3^4) orthogonal array, as suggested by Taguchi.

The numbers in each column indicate the experimental layout or levels of specific factors A-D. These factors are: a) the collimator type, levels 1-3, which are: medium energy high resolution (MEHR), low energy high resolution (LEHR) and low energy all purpose (LEAP), b) the region of interest (ROI) setting of ^{67}Ga gamma spectrum, levels 1-3, which are: the three ranges of the ^{67}Ga decay gamma rays spectrum, c) the scan speed of the gamma camera, levels 1-3 are: the scan speeds of the NaI(Tl) detector head of 80, 120, and 160 mm/min, and d) the activity of the injected ^{67}Ga solution, levels 1-3, which are: the ^{67}Ga activities of 5.55, 7.40 and 9.25MBq.

Table 1. *Standard orthogonal arrays of the nine Groups, following Taguchi's suggestion. The numbers in each column indicate the experimental layout or levels of specific factors A-D*

Group No.	Factor A	Factor B	Factor C	Factor D
1	1	1	1	1
2	1	2	2	2
3	1	3	3	3
4	2	1	2	3
5	2	2	3	1
6	2	3	1	2
7	3	1	3	2
8	3	2	1	3
9	3	3	2	1

These factors are a) the type of the collimator, b) the ROI setting of ^{67}Ga gamma spectrum, c) the scan speed and d) the activity of the injected ^{67}Ga solution.

Analysis of variance

A loss of function [η] measures any deviation between experimental values and desired values. Taguchi recommended the use of a loss function to express deviations of performance characteristics from desired values. The value of the loss function is transformed into a S/N ratio. Performance characteristics fall into three classes, which are: lower-is-better, higher-is-better and nominal-is-best. Each is associated with a particular definition of S/N ratio, which is used in the computation of the optimal combination of factors. A larger S/N ratio always corresponds to a better quality characteristic, regardless the category. The optimal values of operating factors are those values that yield the highest S/N ratio [11]. Therefore, the quality of an image of a planar phantom that is obtained using various gamma camera imaging system settings can be calculated as follows [12]:

$$\eta_i = -10 \log\left[\frac{1}{r}\sum_{j=1}^{r} y_{i,j}^{-2}\right] \quad (1)$$

where η_i is the loss function (S/N unit: *dB*) of the ith group. A larger η is preferable herein, since the quality of a phantom image is higher-is-better. The value $y_{i,j}$ is the judged grade of phantom image of the ith group in the jth trial, and r is the number of trials in each group, which is three herein (the phantom image was graded by three radiologists). SS_{Total}, SS_{Factor}, SS_{error} and DoF (degrees of freedom) are defined as follows,

$$SS_{Total} = \left[\sum_{i=1}^{n}\sum_{j=1}^{r} y_{ij}^2\right] - n \times r \times \bar{\bar{y}}^2 \quad (2)$$

$$SS_{Factor} = \frac{n \times r}{L}\sum_{k=1}^{L}(\bar{y}_k - \bar{\bar{y}})^2 \quad (3)$$

$$SS_{error} = SS_{total} - \sum_{i=1}^{n} SS_{Factor_i} \quad (4)$$

$$DoF_{Total} = n \times r - 1; \quad DoF_{Factor} = L - 1; \quad DoF_{error} = n \times (r - 1) \quad (5)$$

where SS_{Total} is the sum of squares of all variances. y_{ij} is the specific judged grade of phantom image of the ith group in the jth trial, and $\bar{\bar{y}}$ is the average of all the judged grades of phantom image. SS_{Factor} is the sum of squares that correlates with the particular operating factor; $\bar{y}_k$ is the average judged grade that is associated with the specific factor. L and n are the numbers of assigned level of the operating factor and all groups, respectively. The operating factors are: a), b), c) and d), as described before. The corresponding numbers, L and n, are: three and nine, respectively in this study. SS_{error} is the sum of squares of only the random errors. Define F_{factor} as the index in the *F-test* for checking the specific factor and is expressed as,

$$F_{factor} = \frac{SS_{factor}/DoF_{factor}}{SS_{error}/DoF_{error}} \quad (6)$$

where DoF_i is the number of degrees of freedom, and is two for each of the four factors herein. The random error is defined herein as the deviation of the grade given by three radiologists [9X(3-1)= 18] [Eq. 5]. The *F-test,* developed by Dr Fisher (Ronald Aylmer Fisher, 1890-1962) [13], is a test of the assumption that variances of two sampled populations are equal. If the variances are equal, there is only a 1% chance that the value of F will exceed $F_{0.01}$ (the value of $F_{0.01}$ depends on the number of samples taken from each population). Therefore, if $F > F_{0.01}$, it is statistically likely that the variance of one population is larger than the variance of the other. Since SS_{error} is the variance due to random fluctuations and if factor A is likely to influence η then F_A will likely be greater than $F_{0.01}$.

Gamma camera

In routine X-rays diagnosis, patients are passively exposed to external X-rays. In contrast, the acquisition of images using a gamma camera scanning is an active process, since ^{67}Ga-citrate solution is first injected into the human body, from which the decay gamma rays are emitted toward an external NaI(Tl) detector after the ^{67}Ga-citrate solution has been entirely absorbed by the body. Optimizing the settings of the gamma camera imaging acquisition system is crucial to preventing any possible errors in interpreting diagnostic information.

The gamma camera (Siemens E-CAM) was located at Chung-Shan Medical University Hospital (CSMUH). Each of its two NaI(Tl) 480X330X5mm^3 plate detectors was connected to 59 photo multiplier tubes (PMT), with diameters of 50.8mm (2in), to record image. The three types of collimators that were used herein were MEHR, LEHR and LEAP [14]. Table 2 presents the precise specifications of the three collimators. Each collimator was composed of an array of lead grids of various thicknesses that were customized for specific practical purposes. Ideally, any two detectors can capture~60% of the emitted gamma rays. The decay gamma rays that were released from the ^{67}Ga radionuclides in the patient could be recorded and plotted.

Planar phantom

The planar phantom was specifically designed to evaluate the spatial resolution of the gamma ray imaging system. Figure 1 presents the acrylic polymethylmethacrylate (PMMA) planar phantom (200X300X20mm^3) that was utilized herein. As clearly presented in Figure 1 (A), the slits were laser-cut in unique shapes as: (1) intersecting lines, (2) group of parallel lines, (3) eccentric circles and (4) isogonal lines. The machined slits were 1mm wide, and 5mm deep. These unique shapes were chosen to create a series of discrete visible gaps that could help to quantify the spatial resolution of phantom image. Figure 1 (B) presents the real image that was obtained using the gamma camera. As clearly presented in part (B), the tight discrete gaps from the imaging reconstruction of gamma camera were interfered with each other at the bottom of the eccentric circles, so the complexity of the images could be interpreted as part of a volume artifact, leading to a mistaken clinical diagnosis. In this work, the purpose of the optimization is to minimize the size of the artifact (*i.e.* to increase the quality of spatial resolution).

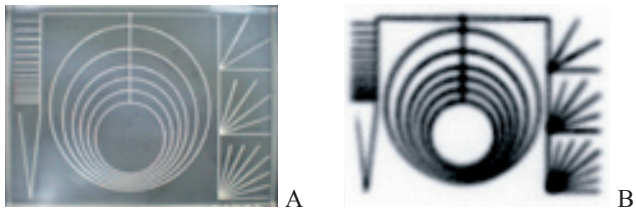
A B

Figure 1. The acrylic polymethylmethacrylate (PMMA) planar phantom (200X300X20mm^3) that was used herein. (A) The slits were laser-cut with unique shapes as: (1) intersection lines, (2) parallel line pairs, (3) eccentric circles and (4) isogonal lines. The machined slits were 1mm-wide, and 5mm-deep from the surface. (B) The real image that was acquired using the gamma camera.

^{67}Ga gamma rays spectrum

The three major energies of ^{67}Ga gamma ray emission were 93.3keV, 184.6keV and 300.2keV; the respective branching ratios of the specific decay gamma ray energy peaks (I_r) were 37.8%, 20.9% and 16.8% following the electron capture by the ^{67}Ga radionuclide. However, since the energy resolution of the NaI(Tl) detector is poorer than that of the HpGe detector, gamma emissions at energies of 91.2keV (I_r: 3%), 208.9keV (I_r: 2.4%) and 393.5keV (I_r: 4.7%) may also be important [15]. Hence, the ROI of the acquired ^{67}Ga gamma rays spectrum was as shown in Table 3.

^{67}Ga-citrate solution and grading

Solutions of ^{67}Ga-citrate with various concentrations, made by Global Medical Solution (GMS), were diluted in 6.0mL of water and then injected into the slits of a planar phantom for scanning. The planar phantom was placed between 30mm above and 50mm below a thick acrylic plate which modeled the body of a patient. Therefore, the total thickness of the assembled set of planar phantom sets was 100mm (30+20+50=100mm). From the planar phantom image, 24-40 counts/pixel were detected, matching closely with the data on real patients obtained in routine nuclear medicine examinations. For example, a solution of ^{67}Ga-citrate solution with a radioactivity of 185MBq was injected into a ~70kg patient. After 3-4h the radioactive solution as distributed in

Table 2. *Precise specifications of the three collimators used*

Collimator	Hole diameter (mm)	Holes no.	Lead grid thickness (mm)	Allowable max. E_r (keV)	Resolution (mm)
LEHR	1.8	30,000	0.3	150	7.4
LEAP	2.5	18,000	0.3	150	9.1
MEHR	3.4	6,000	1.4	400	13.4

Table 3. *The ROI of the acquired ^{67}Ga gamma rays spectrum. The conventional setting of the imaging system in the Chung Shan Medical University Hospital is "level 1" by default*

ROI	93.3keV	184.6keV	300.2keV
Level 1	20%	15%	15%
Level 2	30%	25%	15%
Level 3	20%	15%	0%

the patients' body and data can be collected. The settings of the gamma camera imaging system can be revised using a specially designed planar phantom. Thus, a suitable planar phantom is designed to quantify either spatial resolution or contrast ratio of the gamma ray scintigraph to be evaluated [16-22]. Thus, 14, 30, 30, 59 counts/pixel were acquired from the skeleton, soft tissue, abdomen and liver, respectively, as obtained during a single routine nuclear medicine examination that was performed in a manner consistent with the standard operating protocol of Chung Shan Medical University Hospital, Department of Diagnostic Radiology.

Figure 2 shows: (A) a typical gamma ray image of the 100mm thick planar phantom set. The anterior images were of higher quality than the posterior ones because the thinner acrylic plate (30mm) attenuated gamma emission less than

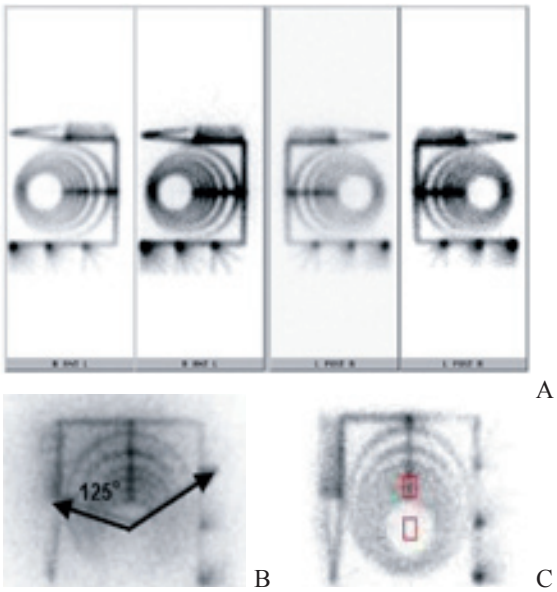

Figure 2. (A) One of the typical gamma ray images of the planar phantom set (100mm thick in total). (B) One doctor estimated the angular expansion of the eccentric circles to be 125 degrees. (C) The hot area was the upper block (the dark) and the cold area was the lower block (the bright). The contrast ratio was the number of pixels quotient in the hot area divided by that in the cold area.

did the thicker one (50mm). The grade of spatial resolution of each planar phantom set image was estimated partially from the angular expansion of the eccentric circles under various settings of the imaging system during optimization. Figure 2 (B) reveals that one doctor estimated the angular expansion of the eccentric circles to be 125 degrees. The angular expansions obtained for each Group of settings were estimated by three highly trained radio-diagnostic doctors. Additionally, the phantom images were randomly presented to the doctors to reduce statistical uncertainty. Figure 2 (C) shows that the contrast ratio between the hot area upper block-the darker and cold area lower block-the bright of the planar phantom set image was another critical quality characteristic in the optimization of the image. The contrast ratio was the number of pixels in the hot area divided by that in the cold area.

Both the angular expansion of the eccentric circles and the contrast ratio between the hot and cold areas of each planar phantom image are: higher-is-better variables. Therefore y_i in Eq. 1 is given by:

$$y_i = w_1 \cdot \frac{\overline{grade}_{1i}}{grade_{1\max}} + w_2 \cdot \frac{\overline{grade}_{2i}}{grade_{2\max}} \quad (7)$$

where $grade_{1i,2i}$ is the average estimated angular expansion or contrast ratio in the *ith* group of setting and $grade_{1\max,2\max}$ is the maximal angular expansion or contrast ratio among all measured data. Both weighting factors w_1 and w_2 were set to 1.0, since both qualities were equally important in the optimization process.

Results

Data analysis

Table 4 presents the combination of factors in the $L_9(3^4)$ orthogonal array, the obtained average grades (Eq. 7), standard deviation (S_d) and S/N [Eq. 1]. The standard deviation was determined from the calculated y_i of each group. Furthermore,

Table 4. *The combination of factors in the $L_9(3^4)$ orthogonal array and the obtained averaged grades [Eq. 7], standard deviation and S/N [Eq. 1]. The standard deviation was determined from the calculated y_i of each group*

Group No.	Collimator	ROI of ^{67}Ga	Scan speed (mm/min)	Activity (MBq)	Avg. grade	Std. Dev.	S/N (η)
1	MEHR	1	80	5.55	1.24	0.17	28.98
2	»	2	120	7.40	1.26	0.15	29.10
3	»	3	160	9.25	1.69	0.24	31.64
4	LEHR	1	120	9.25	0.68	0.07	23.79
5	»	2	160	5.55	0.69	0.10	23.84
6	»	3	80	7.40	1.05	0.08	27.55
7	LEAP	1	160	7.40	0.92	0.12	26.37
8	»	2	80	7.40	0.83	0.13	25.48
9	»	3	120	5.55	1.04	0.11	27.44

Avg: Average, Std: standard, S/N: signal to noise

the mean, S_d and S/N values for each Group were rearranged for each factor. For example, the mean grades of Groups 1, 4 and 7; Groups 2, 5 and 8 and Groups 3, 6 and 9 yielded the contributions of factor B (ROI) at various levels to the quality of the planar phantom set image (Table 1). Figure 3 plots the mean, S_d and S/N against the values of the operating factors of the gamma camera imaging system. Group 3, as indicated in Table 1, had the highest values of any of the Groups. The mean, S_d and S/N for that Group were 1.69, 0.24 and 31.64, respectively. Factors A (collimator) and B (ROI) dominated the quality of the images from the gamma camera imaging system, because the fluctuations in data that were associated with changes in these factors exceeded those associated with fluctuations of the other factors.

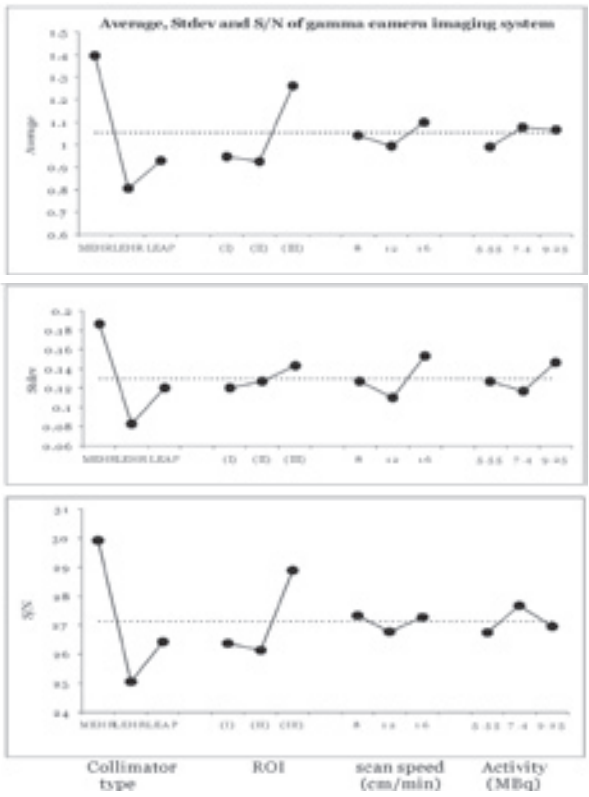

Figure 3. The rearranged average, S_d and S/N against the operating factors of the gamma camera imaging system.

Cross-interaction among factors

Taguchi's method not only yielded the dominant factor, but also effectively elucidated particular cross-interactions among factors. In the unique orthogonal arrangement of various values of factors, the frequencies of the levels were fixed across the nine Groups (Table 1), and the data thus obtained were rearranged to elucidate the cross-interactions among the factors. This arrangement was critical to analyzing the L_9 (3^4) orthogonal array, because the particular data arrangement provided a level III resolution (cross-interactions between factors may be hidden inside other individual factors), as Taguchi pointed out [12]. Figure 4 presents four cross-interactions between pairs of factors. Parts (A), (B), (C) and (D) plot collimator vs. ROI, collimator vs. scan speed, collimator vs. activity and ROI vs. scan speed, respectively, for the gamma camera imaging system.

The three lines in parts (B), (C) and (D) all show strong interactions, revealing that the values of factors C (scan speed) and D (activity) had to be traded-off with that of either factor A (collimator) or factor B (ROI) in level three to optimize performance, and factor A (collimator) dominated all of the factors. Part (A) also exhibits a weak cross-interaction between factor A (collimator) and factor B (ROI), and the S/N is maximized when factors A and B is at level 1 and 3, respectively. Factor A and B, therefore, can be determined individually without interfering the integrated performance. Eventually, the optimal settings of the gamma camera imaging system were determined to be the use of the MEHR collimator, ROI at level 3, a scan speed of 160mm/min and a radioactivity of the ^{67}Ga-citrate solution of 9.25MBq.

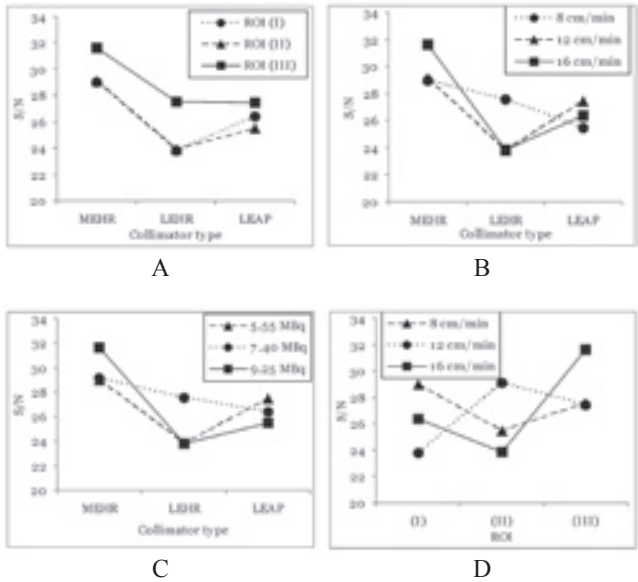

Figure 4. Four cross interactions between pairs of factors. Parts (A), (B), (C) and (D) plot collimator vs. ROI, collimator vs. scan speed, collimator vs. activity and ROI vs. scan speed, respectively, for the gamma camera imaging system.

Analysis of variances, ANOVA

The identity of the dominant factor in the gamma camera imaging system was confirmed by conducting an F-test [Eq. 6]. Table 5 presents the attributed confidence level of particular factors to the effectiveness of the imaging system. An operating factor is regarded to be significant if the corresponding confidence level exceeds 99%. Therefore, (1) collimator type, and (2) ROI of the gamma camera imaging system were the significant factors, because their associated confidence levels were exactly 100%. Furthermore, either factor A (collimator) or factor B (ROI) can be adjusted individually to fulfill the specific requirement, because there is only weak correlation between these two factors (Fig. 4A). Both the scan speed and the activity of the ^{67}Ga radionuclide are regarded as insignificant factors, because their associated confidence levels were 96.0% or 93.6%, respectively. Therefore, neither the scan speed nor the activity of ^{67}Ga can be set to yield the confidence level that is required for clinical diagnosis. Additionally, the activity of ^{67}Ga only from 5.55 to 7.4MBq still slightly upgrades the imaging quality (Fig. 3, the 4th factor). However, the activity of the ^{67}Ga radionuclide can be reasonably reduced according to the ALARA principle, but the two dominant factors collimator, ROI must be considered differently, since they strongly influence the effectiveness of the clinical gamma camera imaging system.

Clinical verification

The optimal factor settings of the gamma camera imaging system that were derived using the planar phantom were verified by performing a routine nuclear medicine examination. The conventional settings of the factors of a gamma camera for the ^{67}Ga-citrate examination are: the use of a MEHR collimator, ROI at level 1, a scan speed of 80mm/min and use of a solution of ^{67}Ga-citrate with a radioactivity of 185MBq. In fact, the optimal settings are: use of a MEHR collimator, but ROI at level 3 (Table 3), a scan speed of 160mm/min and use of a solution of ^{67}Ga-citrate with a radioactivity of 185MBq. The activity of the ^{67}Ga-citrate holds as original setting because the factor ^{67}Ga activity has minor importance and so is set according to the ALARA principle.

Figure 5 compares two typical patients under ^{67}Ga-citrate nuclear medicine examination (case A: male, 57y, sarcoma; case B: female 22y, Behcet's syndrome). In Fig. 5, on the left, the two underwent a ^{67}Ga-citrate whole body examination with the conventional settings, while on the right, the same two patients were examined with the optimal settings. Three highly trained radio-diagnostic doctors agreed that the optimal setting yielded clearer images with greater contrast than did the conventional settings. Specifically, in case A, the uptake lesions in the mediastinum were easily separated and their margins easily delineated. Another two lesions in the splenic fossa were clearly seen, and the clavicles can also be well identified. In case B, the shadow of the ribs and pelvis could be clearly identified, and the sacroiliac joint could also be delineated from the optimal figure. From the optimal diagnostic figure, the urinary bladder and scrotum could be separately identified and the two testes showed an increased uptake. Similar comparisons were made across ten cases, and the same results were obtained in nine of them. All patients provided

Table 6. *The recalculated averages and S/N for each group, based on various combinations of weighting factors. The variation in the preferred settings obtained using various combinations of weighting factors reveals the practical targeting of multiple quality characteristics, although the averages and S/N are still maximized by setting the factor values to group 3 for all combinations of weighting factors herein*

Group No.	$w_{1,2}$: [1.0, 1.0]		$w_{1,2}$: [0.7, 0.3]		$w_{1,2}$: [0.4, 0.6]	
	Avg. grade	S/N (η)	Avg. grade	S/N (η)	Avg. grade	S/N (η)
1	1.24	28.98	0.53	21.52	0.58	22.40
2	1.26	29.10	0.54	21.72	0.62	22.97
3	1.69	31.64	0.79	24.99	0.74	24.44
4	0.68	23.79	0.21	13.38	0.25	15.09
5	0.69	23.84	0.17	11.63	0.20	12.99
6	1.05	27.55	0.37	18.44	0.56	22.00
7	0.92	26.37	0.25	15.21	0.35	18.09
8	0.83	25.48	0.28	16.16	0.40	19.22
9	1.04	27.44	0.37	18.44	0.54	21.75

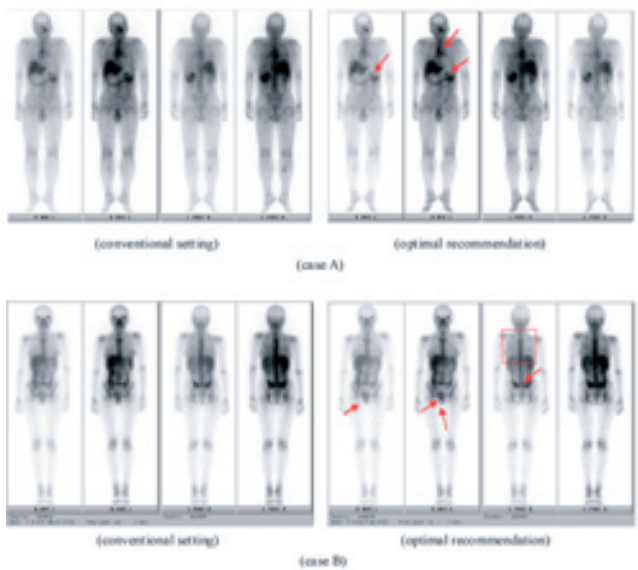

Figure 5. A comparison of two typical patients under ^{67}Ga-citrate nuclear medicine examinations. The two patients as indicated on the left underwent a ^{67}Ga-citrate whole body examination using the conventional settings, while the same two patients as indicated on the right were examined under the optimal settings.

Table 5. *The contributions of particular factors to the effectiveness of the imaging system. An operating factor is regarded to be significant if the percentage exceeds 99%*

Factor	*SS*	*DOF*	*Var.*	*F*	Probability	Confidence level	*Significant
A. Collimator	4.64	2	2.32	121.1	0.0%	100.0%	Yes
B. ROI	1.68	2	0.84	43.8	0.0%	100.0%	Yes
C. Scan speed	0.13	2	0.06	3.4	4.0%	96.0%	No
D. Activity	0.11	2	0.06	2.9	6.4%	93.6%	No
Total	7.77	*Significant: over 99% confidence level					

SS: scan speed, DOF: dominant factors, Var.: variance

written informed consent prior to their inclusion in the testing procedure after thorough explanation of the study. The clinical procedures had been accomplished between August to December, 2009. The optimization of the imaging system improved the gamma camera images for better clinical examination.

Table 6 shows the recalculated means and S/N for all groups, for various combinations of weighting factors.

Discussion

The definition of y_i [Eq. 7] that is used herein can be revised to satisfy various requirements of researchers. The angular expansion of the eccentric circles and the contrast ratio of the planar phantom herein are equally weighted in determining the effectiveness of the imaging system, but the weighting factors can be modified to meet the various requirements of real examinations. Unlike Grey's relational analysis or Fuzzy's analysis, which are applied to multiple quality characteristics [23, 24], Taguchi's optimization was developed to optimize a single quality characteristic. Taguchi's method can be used when either the angular expansion of eccentric circles or the contrast ratio of the planar phantom image is to be determined, but optimizing mutually independent variables is more complex. The choice of weighting factors provides a solution under some conditions. For example, the combination of weighting factors [w_1, w_2] in the S/N calculation can be revised to either [0.7, 0.3] (biased towards angular expansion) or [0.4, 0.6] (biased towards contrast ratio).

The variation in the preferred settings with the combination of weighting factors reveals the practical targeting of multiple quality characteristics, although the means and S/N are still maximized by setting the factor values to Group 3 for all combinations of weighting factors herein (Table 6).

Gamma camera imaging ^{67}Ga quality was optimized using Taguchi's analysis and a planar phantom. A PMMA planar phantom was LASER-cut to form groups of 1mm-wide and 5mm-deep slits to successfully determine both the spatial resolution and the contrast ratio that could be achieved in a ^{67}Ga-citrate nuclear medicine examination. Combinations of values of operating factors for a gamma camera imaging system were set using Taguchi's method. Similar analysis is ongoing in both Chung Shan University Hospital and Buddhist Tzu Chi General Hospital, Taichung, Taiwan to optimize the settings of ^{99m}Tc-MDP nuclear medicine examination. The Taguchi's analysis successfully proves its potential application in optimizing the similar settings for ^{99m}Tc-MDP.

In conclusion, our study with the Taguchi's method showed that for a routine whole body scan with 185MBq of ^{67}Ga-citrate, the optimal factor setting was the use of a MEHR collimator, ROI at level 3, scan speed of 160mm/min and ^{67}Ga dose of only 9.25MBq. The dominant factor was the type of collimator and minor factors were scan speed and activity of ^{67}Ga radionuclide. Taguchi's analysis is most effective in targeting a single quality characteristic.

Acknowledgement
The authors would like to thank the National Science Council of the Republic of China for financially supporting this research under Contract No. NSC 96-2221-E-166 -001 -MY3.

Bibliography

1. Ferretti A, Chondrogiannis S, Marcolongo A et al. Phantom study of a new hand-held (gamma0-imaging probe for radio-guided surgery. *Nucl Med Commun* 2012; doi: 10.1097/MNM.0b013e32835a7ccd
2. Hruska CB, Weinmann AL, O'Connor MK. Proof of concept for low-dose molecular breast imaging with a dual-head CZT gamma camera. Part I. evaluation in phantoms. *Med Physics* 2012; 39: 3466-75.
3. Freek JB, Gerralt AV. Photon-counting versus an integrating CCD-based gamma camera: important consequences for spatial resolution. *Physics Med Biol* 2005; 50(12): N109-19.
4. Boren EL, Delbeke D, Patton JA et al. Comparison of FDG PET and positron coincidence detection imaging using a dual-head gamma camera with 5/8-inch NaI(Tl) crystals in patients with suspected body malignancies. *Eur J Nucl Med* 1999; 26: 379-87.
5. Israel O, Front D, Lymphoma IN et al. *Nuclear Oncology*. Berlin: Springer Verlag, 1999; p185-208.
6. Chen CY, Liu KC, Chen HH et al. Optimizing the TLD-100 readout system for various radiotherapy beam doses using the Taguchi methodology. *Appl Rad and Isot* 2010; 68(3): 481-8.
7. Pan LK, Chou DS, Chang BD. Optimization for solidification of low-level- radioactive resin using Taguchi analysis. *Waste Management* 2001; 21: 762-72.
8. Pan LK, Wang CC, Hsiao YC et al. Optimization of Nd:YAG laser welding onto magnesium alloy via Taguchi analysis. *Optic & Laser Tech* 2004; 37: 33-42.
9. Miyazama S, Lon NH, Tam SC. Application of experimental design in ball burnishing. *Int J Machine Tools Manuf* 1993; 33(6): 841-52.
10. Loh NH, Miyazawa S, Lee SSG et al. An investigation into ball burnishing of an aisi 1045 free-form surface. *J Mater Process Technol* 1992; 29: 203-11.
11. Taguchi G. *Introduction to quality engineering*. Asian Productivity Organization Tokyo 1990.
12. Phadke MS. *Quality engineering using robust design*. Prentice Hall, Englewood Cliffs, New Jersey 1989.
13. Fisher RA. *Design and analysis of experiments*. Olive and Boyd. London 1925.
14. Jackson SA. *Gamma Camera*, 2008; http://www.radiologyphysics.bitica.com/files/Microsoft%20PowerPoint%20-%20Gamma%20Camera.ppt.pdf
15. Lederer CM, Shirley VS. *Table of isotopes*. Wiley-interscience Publishing Co. New York 1978.
16. Seret A. Hot and cold contrasts in high-resolution ^{99m}Tc planar scintigraphy: A survey of fifty-two camera heads using the PICKER thyroid phantom. *Physics Medica* 2010; 26: 166-72.
17. Lees JE, Bassford DJ, Blackshaw PE et al. Design and use of mini- phantoms for high resolution planar gamma cameras. *Appl Rad and Isot* 2010; 68: 2448-51.
18. Pani R, Soluri A, Scafe R et al. A compact gamma ray imager for oncology. *Nucl Instru & Meth In Phys Res A* 2002; 477: 509-13.
19. Pani R, Cinti MN, Pellegrini R et al. Compact large FOV gamma camera for breast molecular imaging. *Nucl Instrum & Math in Phys Res A* 2006; 569: 255-9.
20. Kieper D, Majewski S, Kross B et al. Optimization of breast imaging procedure with dedicated compact gamma cameras. *Nucl Instrum & Meth in Phys Res A* 2003; 497: 168-73.
21. Giokaris ND, Loudos GK, Maintas D et al. Imaging of breast phantoms using a high-resolution position sensitive photomultiplier tube. *Nucl Instrum & Math in Phys Res A* 2003; 497: 141-9.

22. Hruska CB, O'Connor MK. Molecular breast imaging A phantom study on the impact of collimator selection on the detection of sub- 10mm breast lesions. *Nucl Instrum & Math in Phys Res A* 2006; 569: 250-4.
23. Pan LK, Wang CC, Shih YC et al. Optimizing multiple qualities of Nd:YAG laser welding onto magnesium alloy via grey relational analysis. *Science and Techm of Welding and Joining* 2005; 10(4): 503-10.
24. Pan LK, Wang CC, Wei SL et al. Optimizing multiple quality characteristics via Taguchi method-based Grey analysis. *J Mater Process Technol* 2007; 182: 107-16.

Thomas Rowlandson (Great Britain)-1756: Dissecting Room. Handmade lithography.